

A toxicity assessment of hydroxyapatite nanoparticles on development and behaviour of *Drosophila melanogaster*

S. Aurosman Pappus · Basanti Ekka ·
Swetapadma Sahu · Debabrat Sabat ·
Priyabrat Dash · Monalisa Mishra

Received: 4 January 2017 / Accepted: 8 March 2017 / Published online: 6 April 2017
© Springer Science+Business Media Dordrecht 2017

Abstract The effects of oral intake of hydroxyapatite nanoparticles (HApNPs) were investigated on growth, development and behaviour of *Drosophila*. The *Drosophila* responses to various concentrations of HApNPs were compared. At lower concentrations, i.e. 5 mg L⁻¹ more amount of oxidative stress was produced than that of highest concentration, i.e. 80 mg L⁻¹. The increased amounts of oxidative stress reflect a higher amount of ROS production and increased cell damage within the larval gut. HApNPs was further shown to interfere with the calcium and phosphorus absorption pathway. Besides all these damage, HApNPs causes developmental delay in the late third instar larvae. The most significant anomaly was observed in pupae count, fly hatching after the feeding of HApNPs. Flies hatched from treated vials have decreased body weight with defective walking behaviour. Hatched flies have a phenotypic defect in the wing, eye and thorax of the bristles. Along with

these changes, the adult fly becomes more prone towards stress. The findings hint that HApNPs persuade noxious effects and alter the development, structure, function and behaviour of the fly in a concentration-dependent manner.

Keywords Hydroxyapatite nanoparticles · Mechano-sensory neurons · *Drosophila melanogaster* · Oxidative stress · Micronuclei · Phosphorus absorption · Environmental and health effects

Introduction

Nanotechnology, from a decade or two, has become one of the most widely used technique in pharmaceutical, biomedical and cosmetics as well as photothermal therapy (Reddy et al. 2012). Having tunable size, larger surface area and label-free characterization methods allow the wide use of nanoparticles (NPs) in various fields (Albanese et al. 2012). Some of the NPs like silica nanoparticles and solid lipid nanoparticles (SLN) are used as drug carriers to target specific cells in cancer therapy and directed drug delivery (Cho et al. 2008b; Slowing et al. 2008; MuÈller et al. 2000; Cho et al. 2008a). Hydroxyapatite nanoparticles (HApNPs) have extensive applications in the field of medicine by virtue of its good biocompatibility and bioactivity (Kantharia et al. 2014). It has a hexagonal structure with a Ca/P proportion 1.67, which is matching with bone apatite (Mostafa and

Electronic supplementary material The online version of this article (doi:10.1007/s11051-017-3824-8) contains supplementary material, which is available to authorized users.

S. A. Pappus
Department of Biological Sciences, IISER Kolkata, Haringhata
Farm, Nadia, West Bengal 741252, India

B. Ekka · P. Dash
Department of Chemistry, National Institute of Technology,
Rourkela, Odisha 769008, India

S. Sahu · D. Sabat · M. Mishra (✉)
Department of Life Science, National Institute of Technology,
Rourkela, Odisha 769008, India
e-mail: mishramo@nitrkl.ac.in

Brown 2007; Kalita et al. 2007). Along with that, it is thermodynamically stable under various physiological conditions such as temperature and pH (Kalita et al. 2007). Its stability and biocompatibility allow it to be used in implanting, coating, bone filling, bone substitutes and oral treatment (Sun et al. 2001; LeGeros 1991). Despite having vast applications, the toxicity of hydroxyapatite nanoparticles has been reported in zebrafish (*Danio rerio*), where HApNPs cause axial deformation as well as developmental delay (Zhao et al. 2013b). In osteoblasts-like cells, HApNPs (a naturally occurring calcium apatite) can induce proliferation and apoptosis (Shi et al. 2009). The toxicity reported from HApNPs is alarming and warrants a thorough investigation using a model organism.

Several studies used *Drosophila* as a model system to learn the detriment caused by nanoparticles. Toxicity of silver nanoparticles was assessed where silver nanoparticles cause oxidative stress, DNA damage, apoptosis and heat shock stress in *Drosophila*. Silver NPs further resulted in developmental delay and lesser developmental success (Ahamed et al. 2010; Gorth et al. 2011). *Drosophila* treated with silver and cobalt nanoparticles have a phenotypic defect like abnormal wing spots and bristles (Demir et al. 2011; Vales et al. 2013). Gold nanoparticles affect the fertility and development by causing altered phenotypes in bristle, eye and wings. Gold nanoparticle-treated flies show DNA fragmentation, oxidative stress and early apoptosis accompanying with it (Vecchio et al. 2012; Pompa et al. 2011). Silica nanoparticles cause membrane destabilization and mitochondrial membrane potential loss in the gut cells of *Drosophila* along with increased oxidative stress and caspases activation, ultimately leading to cellular apoptosis (Pandey et al. 2013). Most nanoparticles such as sodium and gold can penetrate the cellular membrane easily due to its small size, hence cause toxicity to cells. However, it is also reported that nanoparticles like cerium oxide moderate free-radical reconciled toxicity in *Drosophila* cells (Cohen et al. 2008).

Besides nanoparticle toxicity study, *Drosophila* has long been used to study several neurodegenerative diseases like Alzheimer's disease and seizure disorders (Ong et al. 2015; Pandey and Nichols 2011). Low maintenance cost, short life cycle and all the well-studied developmental stages make it an ideal model to study the toxic effect of any chemical (Campos-

Ortega and Hartenstein 2013). It has only four chromosomes and 75% genes of the *Drosophila* genome share functional homology with the human disease-causing genes (Pandey and Nichols 2011). More importantly, HAp, a nidus material for mineral deposition is conserved from *Drosophila* to human being (Duer et al. 2008; Dorozhkin 2010; Evan et al. 2008; Ma et al. 2011). Many studies used *Drosophila* to understand the mechanism of mineralization (Jiang et al. 2006; Ryall 2008). The pathogenesis of kidney stone was deciphered by using *Drosophila* model (Chen et al. 2011; Hirata et al. 2012) since both *Drosophila* and human kidney stone possess hydroxyapatite as the main composition (Evan 2010). Furthermore, Chi et al. (2015) proved the mechanism of ectopic calcification using *Drosophila* (Chi et al. 2015). All these studies hints that various metabolic pathways involved in the calcification process is conserved. Hence, *Drosophila* can be used as a model to check the toxicity of HApNP.

Compelling the extensive application of HApNP into contemplation, the aim of this work is to explore the toxic effect of HApNP on development, behaviour and cellular physiology of *Drosophila* when exposed through oral route, which was not investigated in earlier studies.

Material and methods

Fly rearing The fly media used for rearing flies consists of sucrose, cornmeal, yeast powder and agar-agar (type 1). Propionic acid and Nipagin M were added to prevent mould and fungal contamination. The flies were incubated at 25 °C temperature, 60% relative humidity (RH) and were exposed to a 12-h dark-light cycle. The flies used were of Oregon-R type and obtained from C-CAMP Bangalore.

Materials

Orthophosphoric acid, sodium hydroxide, hydrogen peroxide, ammonium hydroxide, calcium hydroxide, 2,7-dichlorofluorescein, trypan blue, nitro blue tetrazolium and hydrochloric acid were purchased from Himedia. All chemicals used in this study were of analytical grade. All the chemicals used in the experiment were as supplied by the company without any further purification.

Synthesis of hydroxyapatite

For the production of unadulterated hydroxyapatite (HAp, 37 gmCa (OH)_2) was liquefied in 100 mL of water. Next, H_3PO_4 was supplemented to get a proportion of Ca/P of 1.67. The pH of the mixture was maintained 10 by the addition of NH_4OH . The resulting product was imperilled to microwave radiation with a machining power of 800 W for 20 min. A precipitate was achieved as a product of the previous step. The precipitate was rinsed several times with distilled water to take away undesirable water-soluble ions. After washing, the desired product is calcined at 500°C for 3 h. The anticipated product was grinded with the help of mortar and pestle to achieve pure hydroxyapatite.

Characterization of NPs

FTIR spectroscopy (PerkinElmer) was used to define the functional groups present in the synthesized HAp. The crystallinity of the produced HAp was scrutinized by an x-ray diffractometer (XRD-PHILIPS PW 1830) with $\text{CuK}\alpha$ source. The morphology of the HAp was explored by field emission scanning electron microscopy (FESEM); successively, the chemical composition was restrained by EDX in Nova NANOSE/FEI. Surface area of the HAp was deliberated by using the Brunauer–Emmet–Teller (BET) equation in QUANTACHROME AUTOSORB (IQ) model ASIQM0000-4. The distribution of pore size and volume were obtained by applying the Barrett–Joyner–Halenda (BJH) method. HApNPs were degassed in vacuum at 150°C . Transmission electron micrographs (TEM) (PHILIPS CM 200) of HApNPs were taken on carbon-coated copper grids. For the zeta potential, the hydroxyapatite nanoparticles were first dispersed in Milli-Q water and sonicated for 20 min. Then, the zeta potential was measured by Malvern NANO-ZS-90.

Treatment For the experiments, the setup consisted of one control having untreated flies and five setups of hydroxyapatite-treated flies of concentration 5, 10, 20, 40 and 80 mg L^{-1} . Hydroxyapatite NPs were sonicated for half an hour in distilled water prior to the experiment to disperse properly. Afterwards, the desired concentration was added to the food. Later five females and three males were transferred to each vial.

Life cycle The flies were transferred to vials containing hydroxyapatite in the food. The flies will feed and lay eggs on the food. The time taken to develop from egg to third instar larvae, from third instar larvae to pupae and to adult was noted. Also, the number of pupae formed and the fraction of pupae hatched into adult flies were noted everyday (Panacek et al. 2011).

Larva crawling behaviour For larvae crawling behaviour, six third instar larvae were taken from each concentration including the control. Larvae were allowed to crawl on a circular surface made from 2% agarose (Nichols et al. 2012). The background was kept black so that it would be easy to distinguish the white larvae. The crawling was recorded by a camera and kept for analysis. The tracking was done by a software named ‘Ctrax: The Caltech Multiple Walking Fly Tracker’ and further analysis and plotting were done by MATLAB (R2015a). Finally, the speed of larvae was calculated in millimeters per second.

Nitro blue tetrazolium assay Larvae from different concentrations including control were subjected for nitro blue tetrazolium (NBT) assay. Briefly, 15 third instar larvae were taken from each vial. Larvae were ruptured with a sterilized needle and the haemolymph was extracted. The extraction was done in cold chamber in order to prevent melanisation of the haemolymph. Five microliters of haemolymph was taken and $10 \mu\text{L}$ of 1X PBS was added to it. This step was followed by the addition of $15 \mu\text{L}$ of 1.6 mM NBT solution. The sample was kept for 1-h incubation in dark. With the onset of incubation, equal volume 100% glacial acetic acid was added to stop the NBT reaction, which was followed by centrifugation. Next, $150 \mu\text{L}$ of 50% glacial acetic acid was added and the absorbance was taken at 595 nm (Jambunathan 2010).

Trypan blue staining Trypan blue staining was done following the given protocol (Krebs and Feder 1997; Carmona et al. 2015). Briefly, six third instar larvae from different vials were isolated and washed in 1X PBS solution in order to remove any traces of food from the surface of the larvae. The larvae were dipped in trypan blue solution (0.02%) and kept on a shaker for 30 min. The excess trypan blue was removed from the larvae surface by washing with 1X PBS solution. Now, the larvae were observed under a stereomicroscope and imaged to check if there was any cell damage.

SEM and EDX Six guts from each concentration were isolated in 4% PFA and kept at 4 °C. Guts were washed with PBS to remove the excess of PFA. Guts were dehydrated by graded serial dehydration process by increasing the concentration of ethyl alcohol. Finally, the dehydrated guts were smeared with a layer of platinum and perceived under scanning electron microscope (SEM) (Nova NANOSEM). The amount of calcium and phosphate were checked from EDX analysis.

Larva gut staining Third instar larvae gut were dissected and kept in 4% paraformaldehyde (PFA) at 4 °C. For staining, guts were rinsed with PBS for 10 min to remove excess PFA. Afterward, PBS was removed and the same amount of PBST was added and kept for 10 min. The addition of PBST was repeated thrice. Subsequently, 2,7-dichlorofluorescein (a marker for ROS) was added and guts were incubated in dark for 30 min as the dye is light-sensitive. Lastly, the guts were eroded with PBS and mounted with mounting media containing DAPI.

Adult climbing assay For the climbing assay, 30 adult flies were isolated from each vial and transferred to a 100-ml measuring cylinder having a mark up to 10 cm. The mouth of the cylinder was closed by a cotton plug. Then, the cylinder was tapped two to three times so that all the flies would come down to the bottommost of the cylinder. Now the flies were permitted to ascend for 10 s. The number of flies that were able to climb up to the 10-cm mark and those which stayed at the bottom was noted (Nichols et al. 2012). This experiment was repeated for six times and the mean value was calculated.

Adult phenotype For phenotypic analysis, 50 flies from each vial were observed under a stereomicroscope. Flies were checked for abnormality in eyes, bristles and wings. The percentage of abnormalities were represented statistically.

Adult weight For weight measurement, 50 adult flies containing 25 males and 25 females were collected from each experimental vial. The weight of 50 flies from each concentration was measured. The average weight for each vial was calculated and plotted in a graph.

Adult H₂O₂ assay For H₂O₂ assay, the adult flies were fed with a paper soaked in a mixture of 6% sucrose and 9% hydrogen peroxide. Then they were observed in an interval of 2 h till flies were left alive.

Statistical analysis

All experiments were reiterated three times and the statistical values (unpaired *p* test) were analysed using Graph pad prism 6.0 software. All the values were compared statistically against the control.

Results

Material characterization

To check the functional groups in the synthesized material, the samples were evaluated by FTIR spectrum (Fig. 1a). The spectra retain sharp and strong band at 3451 cm⁻¹, conforming to stretching mode of OH group, while the peak at 1653 cm⁻¹ corresponds to bending vibration of OH group. Strong bands at 1051, 880 and 579 cm⁻¹ were due to PO₄³⁻ group. The bands obtained for PO₄³⁻ and OH groups in HAp, were in good agreement with other published data (Chaudhry et al. 2006; Yao et al. 2003; Puvvada et al. 2010). A sharp band at 1412 cm⁻¹ was due to CO₃²⁻, which might be incorporated to HAp from the atmosphere during the sample preparation. Since carbonates are the constituents of bone tissues, the presence of CO₃²⁻ may contribute to a vibrant role towards the bioactivity of the synthesized NP. The synthesized NPs were further analysed with x-ray diffraction (XRD) patterns as shown in Fig. 1b. All the diffraction peaks of the HApNPs can easily be catalogued to the pure hexagonal phase of HAp, which counterparts with the JCPDS card no. 09-0432. XRD pattern reveals the crystalline nature of the material.

The synthesized NPs were checked for their structure under FESEM. FESEM image of HAp reveals the rod-like a structure of the prepared material with agglomeration (Fig. 1c). The rod-like structure is further confirmed by TEM image which is shown in (Fig. 1d). Agglomeration in HAp is clearly visible, which is endorsed for large surface area and energy associated with HAp. The size of the hydroxyapatite nanorods were measured from the TEM micrographs using the Image J software. The average length of the HAp rod seems to vary between 70 and 80 nm, while the average diameter was found to be between 40 and 50 nm. The histogram shows an average size of 85 ± 5 nm for the nanoparticles. Moreover, the crystallinity is blameless, and the growth was identical to the rod-like structures as stated in various literature. The lattice fringe was found to be 0.34 nm,

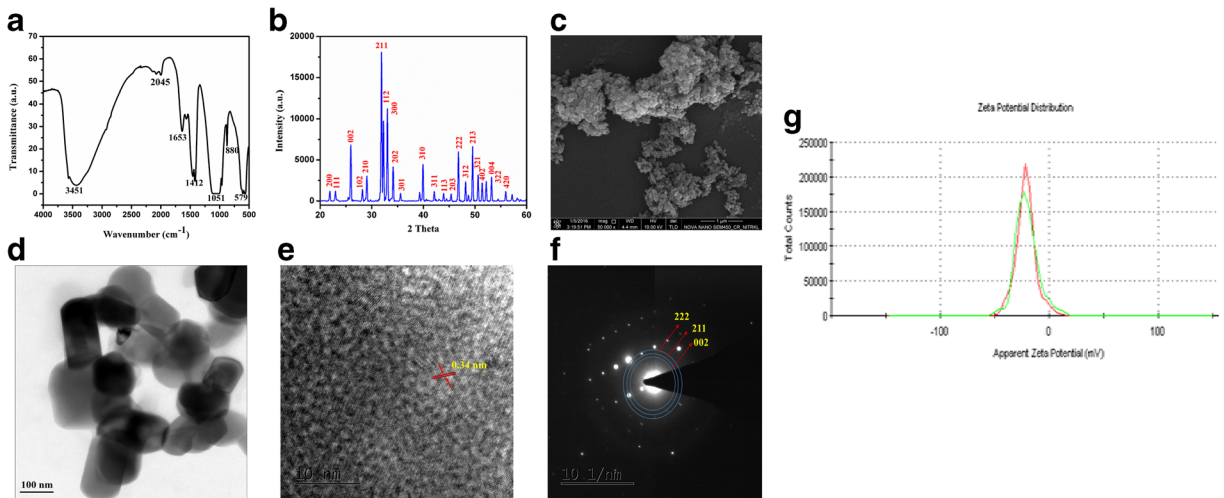


Fig. 1 Characterization of nanoparticles **a** FTIR spectra, **b** XRD pattern, **c** FESEM image, **d** TEM image, **e** HRTEM image, **f** SAED pattern of hydroxyapatite nanoparticles, and **g** zeta potential distribution curve of hydroxyapatite nanoparticles

which corresponds to lattice constants of (002) plane (Fig. 1e). This explains the elevated intensity in the XRD in 002 reflections (Fig. 1b). The above results are consistency with other reported literature for rod-like the structure of HAp. The selected area electron diffraction (SAED) patterns of the HApNP reveal the crystalline nature of the material. The SAED lattice fringes corresponds to the (002), (211) and (222) faces of HAp (Fig. 1f).

To learn about the surface charge and steadiness of the nanoparticles, zeta potential was measured. The dispersant used was Milli-Q water and the temperature was 25 °C. The zeta potential value was found to be -21.6 mV (Fig. 1g). This value signifies that the nanoparticles are moderately stable in the dispersant medium. So agglomeration might only happen when a higher concentration of the nanoparticles is present in the dispersion medium.

Larva crawling behaviour The larvae crawling assay was accomplished to observe the amount of confusion in the crawling behaviour of the third instar larvae. This corroborates the extent of neuronal damage occur in an early developmental stage (Dominick and Truman 1986). The crawling speed of the control larvae was $1.342 \pm 0.03 \text{ mm s}^{-1}$ ($=8.052 \text{ cm min}^{-1}$). With the increase of hydroxyapatite concentration, the average crawling speed decreased. In 5 mg l^{-1} , the speed was $1.123 \pm 0.05 \text{ mm s}^{-1}$ ($=6.738 \text{ cm min}^{-1}$), which ultimately decreased to $0.9450 \pm 0.03 \text{ mm s}^{-1}$ ($=5.67 \text{ cm min}^{-1}$) in the case of 80 mg l^{-1} (Fig. 2a). The larvae tracking paths are demonstrated in Fig. 2b.

Trypan blue staining Trypan blue stains only the dead cells. So, it is possible to distinguish between dead and alive cells. Positive trypan blue staining was seen in 5, 10, 20 and 40 mg l^{-1} . In 5 and 20 mg l^{-1} , prominent staining was seen whereas mild stain was observed in 10 and 40 mg l^{-1} . The damaged cells which took up the blue stain are marked by the dotted circle (Fig. 2c).

NBT assay NBT assay was done to govern the extent of ROS produced in the hemolymph of third instar larvae. In control, the absorbance value at 595 nm was found to be 0.21. In 5 mg l^{-1} , the value increased to 0.286 ± 0.0037 . In 10 mg l^{-1} , the absorbance was 0.249 ± 0.019 and for 20 mg l^{-1} , the absorbance was 0.265 ± 0.018 . In 40 mg l^{-1} concentration, the absorbance was 0.291 ± 0.014 and for 80 mg l^{-1} , the absorbance was 0.224 ± 0.0023 . For NBT assay, the absorbance is directly proportionate to the amount of ROS produced and ultimately corresponds to the extent oxidative damage to the cells. The amount of increase occur with respect to control are plotted in graphs (Fig. 2d).

SEM and EDX Scanning electron microscopy was done in order to determine the amount of calcium and phosphorus within the gut of third instar larvae. In control, the calcium percentage in the gut was 2% and that of phosphorus was 35%. In 5 mg l^{-1} -treated vial, the calcium amount was negligible and phosphorus was 7%. In case of 10 and 20 mg l^{-1} also, there was a negligible amount of calcium whereas phosphorus

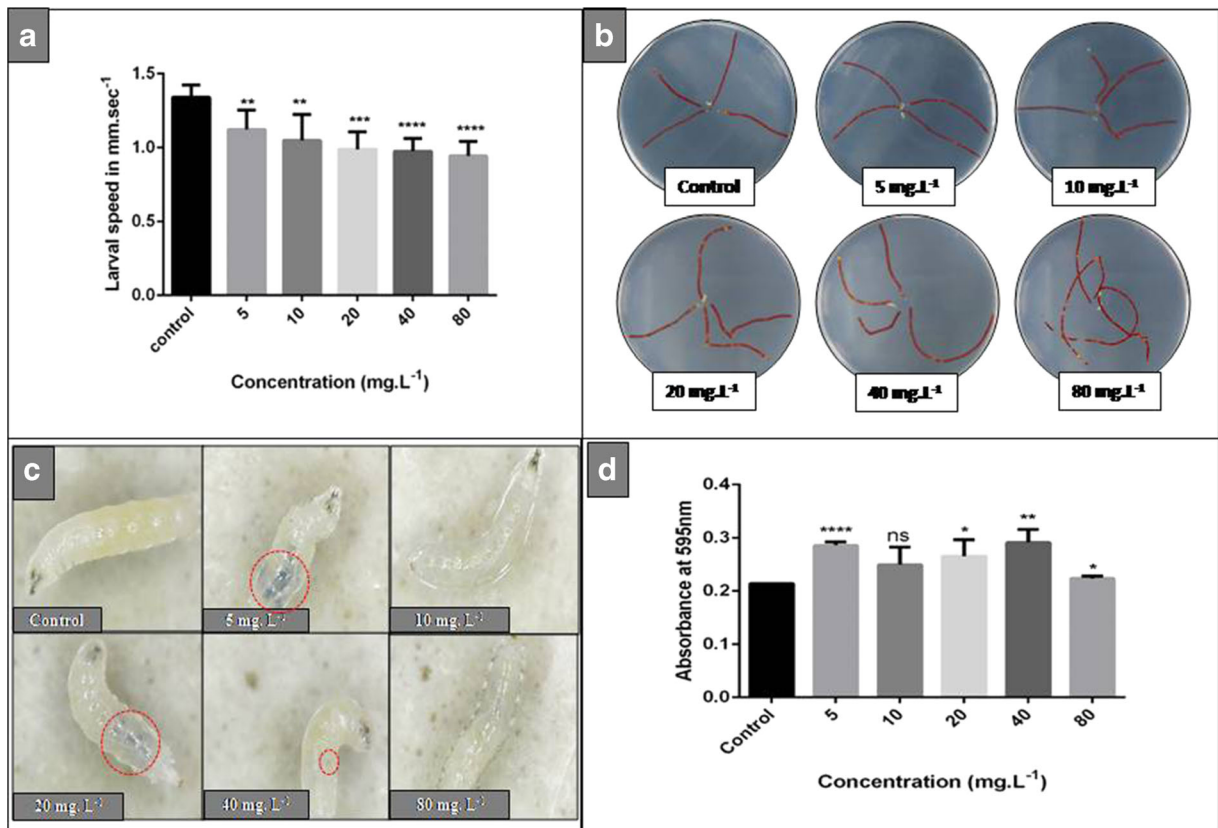


Fig. 2 Assessment of toxicity in third instar larvae. **a** Graphical illustration of the distances travelled by the larvae in different concentrations of HApNPs (mean \pm S.D.) with the significance values against control are represented as asterisk ($n = 30$; ** P value = 0.0042, *** P value = 0.001, **** P value \leq 0.0001). **b** Tracking path of larva crawling. **c** Trypan blue staining to mark any damage in the gut. Red circle indicates the damaged part of the

gut. **d** NBT assay from hemolymph to measure the amount of free radicals in the third instar larvae. The graphs are plotted against the respective concentration of HAp nanoparticles present in the food. The level of significance are marked in comparison to control with asterisks (* P value = 0.0142, ** P value = 0.0056, **** P value $<$ 0.0001, NS P value = 0.1409)

amount was 14.2 and 5.82%, respectively. In 40 mg L⁻¹-treated vial 1.29% calcium and 7.7% phosphorus was found and in 80 mg L⁻¹ treated vial the calcium and phosphorus level found to be 6.89 and 8.0%, respectively (Fig. 3).

Larva gut staining The gut of the third instar larvae was stained with DAPI to check the nuclei of the gut. Except for control, the nuclear damage was seen in all the treated vials. There were instances of clustered micronuclei dispersed all over the gut. Most amounts of these broken nuclei were seen in case of 20, 40 and 80 mg L⁻¹. The nuclei of different concentrations including control are represented in Fig. 4a–f. The amount of ROS was further measured from gut using 2,7-dichlorofluorescein dye. The intensity of the dye indicates the extent of stress level (Fig. 4g–l).

Life cycle The life cycle of eggs hatched in the experimental vials was monitored to analyse if there was any developmental defect. For the same, the time taken from egg to third instar larval stage was recorded. In control, the time was taken to form third instar larvae were about 72 h, whereas in 5, 10 and 20 mg L⁻¹, the time taken was around 84 h. In 40 mg L⁻¹, the time taken for the third instar larvae was around 90 h and for 80 mg L⁻¹, the duration was about 96 h (Fig. 5a).

Percentage of pupae formed A number of pupae was counted to check for any developmental defect due to which fewer pupae could form. The obtained data was normalized so that the total number of pupae in control would be 100 and all the other data were obtained with respect to the control. In 5 mg L⁻¹, the number of pupae hatched was 86.40 ± 1.84 and in 10 mg L⁻¹, it was

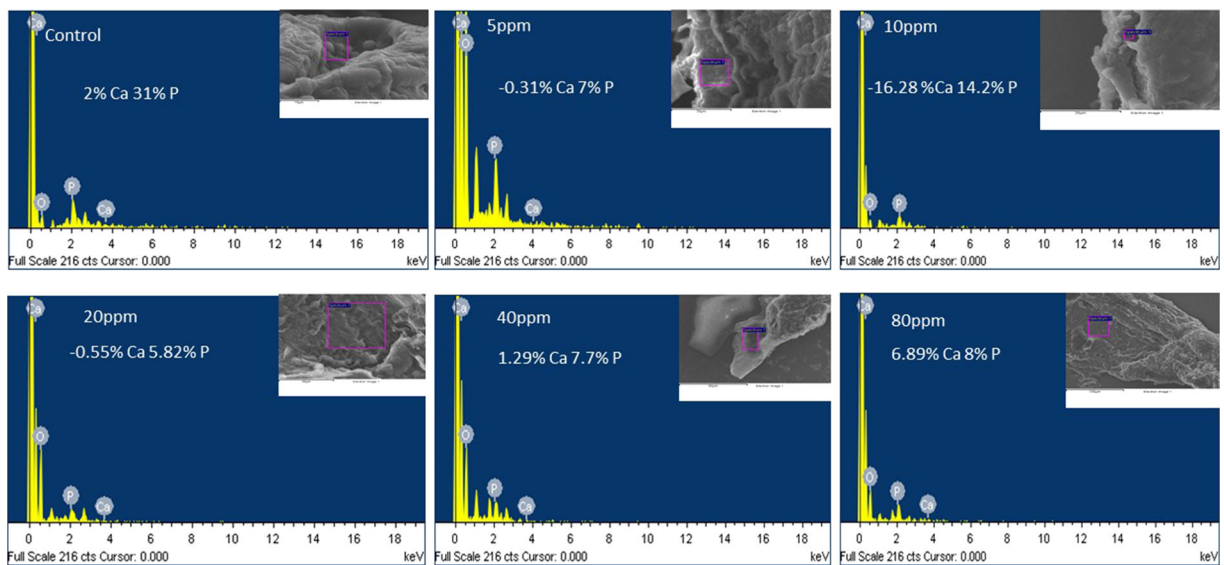


Fig. 3 SEM analysis of gut of third instar larvae EDX analysis of gut of control as well as various concentrations of HApNPs-treated third instar larvae depicting the amount of calcium and phosphorus within the gut

95.01 ± 0.8926 . For 20 mg L^{-1} , the obtained number was 83.76 ± 2.48 . For 40 and 80 mg L^{-1} concentration, the pupae count was 82.50 ± 2.01 and 73.75 ± 3.33 , respectively. The numbers of pupae are plotted as graph (Fig. 5b).

Percentage of adult flies The number of adult flies hatched from pupae was counted from all the vials. All flies hatched from the control were normalized to 100. Number of flies hatched from other vials was compared with respect to the control. In 5 mg L^{-1} -treated vial, the number of adult flies was 87.35 ± 4.11 . In 10 mg L^{-1} , the number was 93.15 ± 0.8072 ; also for 20 mg L^{-1} , the number of adult flies was 86.42 ± 2.647 . In higher concentrations like 40 and 80 mg L^{-1} , the value was 85.85 ± 1.625 and 66.48 ± 4.652 , respectively (Fig. 5c).

Adult weight The weight of the adult flies was calculated from different vials to check the body growth and size. The weight of 50 (1:1 ratio male and female) control flies was found to be 19.5 mg whereas in 5 mg L^{-1} , it was $16.85 \pm 0.492 \text{ mg}$. Likewise, the weight of 50 flies was $17.89 \pm 0.020 \text{ mg}$. For 10 mg L^{-1} , it was $17.47 \pm 0.1745 \text{ mg}$ and for 20 mg L^{-1} , the value was $16.85 \pm 0.043 \text{ mg}$. In 40 mg L^{-1} , the value was $18.49 \pm 0.236 \text{ mg}$ for 80 mg L^{-1} were compared to control, the 80 mg L^{-1} data was non-significant. The body weight was plotted in the form of a graph (Fig. 5d).

Adult climbing assay Climbing assay denominates the behavioural changes that occur in the flies with respect to gravity. This assay is analysed by the number of flies that were able to climb up to the 10-cm mark in the time interval of 10 s. The number of flies that could climb up to 10 cm in control vial was normalized to 100% in due course of time. In 5 mg L^{-1} , $84.31 \pm 3.15\%$ of flies were able to climb whereas $90.06 \pm 0.46\%$ in 10 mg L^{-1} , $89.23 \pm 0.62\%$ in 20 mg L^{-1} , $86.33 \pm 2.46\%$ in 40 mg L^{-1} and $80.74 \pm 0.61\%$ in 80 mg L^{-1} were able to climb up to the 10-cm mark. The result of the climbing assay is plotted in the form of a graph (Fig. 5e).

Adult phenotype

In the HApNP treated flies, abnormalities were found in bristles, eyes and wings.

Wings The wing characteristics like venation and size of the wings were observed in the adult files. In 5 mg L^{-1} -treated vial, the posterior cross vein (PCV) was not continuous thus indicating incomplete venation. In 10, 40 and 80 mg L^{-1} dark patches were observed comprising of comparatively thick hairs on the wing surface. The size and number of the patches increase with increase in treated concentration of HAp. All the phenotypic variations are represented in figures (Fig. 6a). Statistical analysis of the abnormal wings were represented in S1.

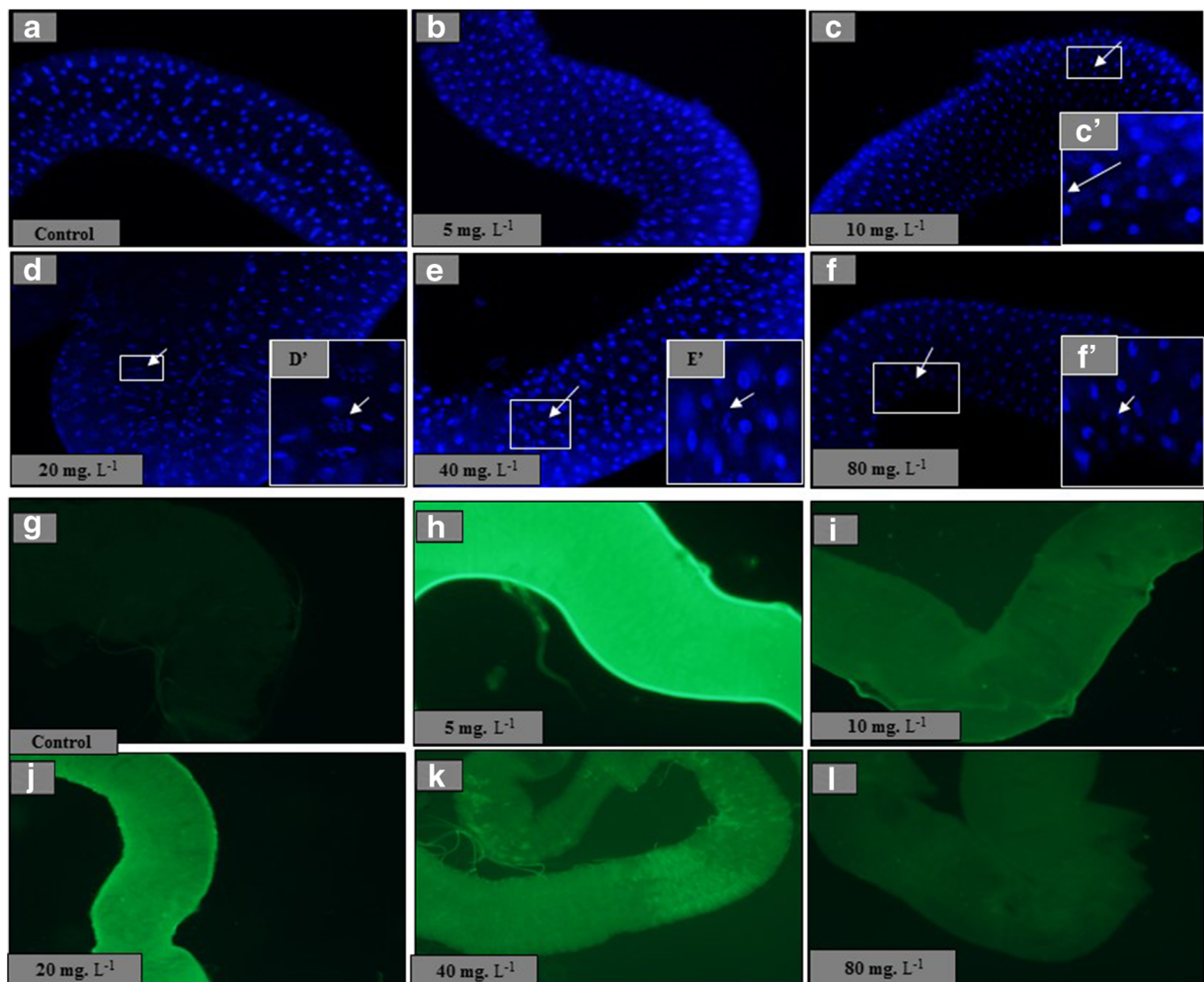


Fig. 4 Fluorescence imaging of gut of third instar larvae (a–f). Guts were stained with DAPI and observed under fluorescent microscope. Nucleus damage was seen in all the cases except the control. c–e More number of damaged nuclei were observed in

comparison with control. The magnified image of the damaged nuclei are shown in the inset (c'–f'). Guts were stained with 2,7-dichlorofluorescein dye to detect the amount of ROS generated within the gut

Bristles The bristles of all the adult flies were observed to find any abnormality which could affect their sensation. In 5 mg L^{-1} , there were a loss of left aSC, pSC and left aDC bristles. Ten milligrams per litre showed loss of right aDC, pDC and both the left-right pSC bristles. In 20 mg L^{-1} , there was no right pSC bristle. Forty milligrams per liter showed loss of left aDC bristle. In 80 mg L^{-1} , there was broken pSC bristle. All the bristle phenotypes from different concentrations are depicted in Fig. 6b. Statistical analysis of the abnormal bristles were represented in S1.

Eyes The external structure of the eye of adult flies was observed to check for any abnormality. In 5 ppm, dark

patches were found and small eye phenotype was seen in all the treated flies. In 10 mg L^{-1} , rough-eye phenotype along with blisters was observed. In 20, 40 and 80 mg L^{-1} , irregular margin in the eye was found indicating missing ommatidia from the boundary. The eye phenotypes are illustrated in Fig. 7. Statistical analysis of the abnormal eyes were represented in S1.

Adult H_2O_2 assay The H_2O_2 assay was done to determine the ability of the adult flies to endure stress. Ten adult flies from each treated vials were given H_2O_2 as food and a number of survivors were noted down till 14 h after the experiment started. Various treated flies were compared with control to measure their stress

resistant property. The survivability was plotted in the form of graphs (Fig. 8).

Discussion

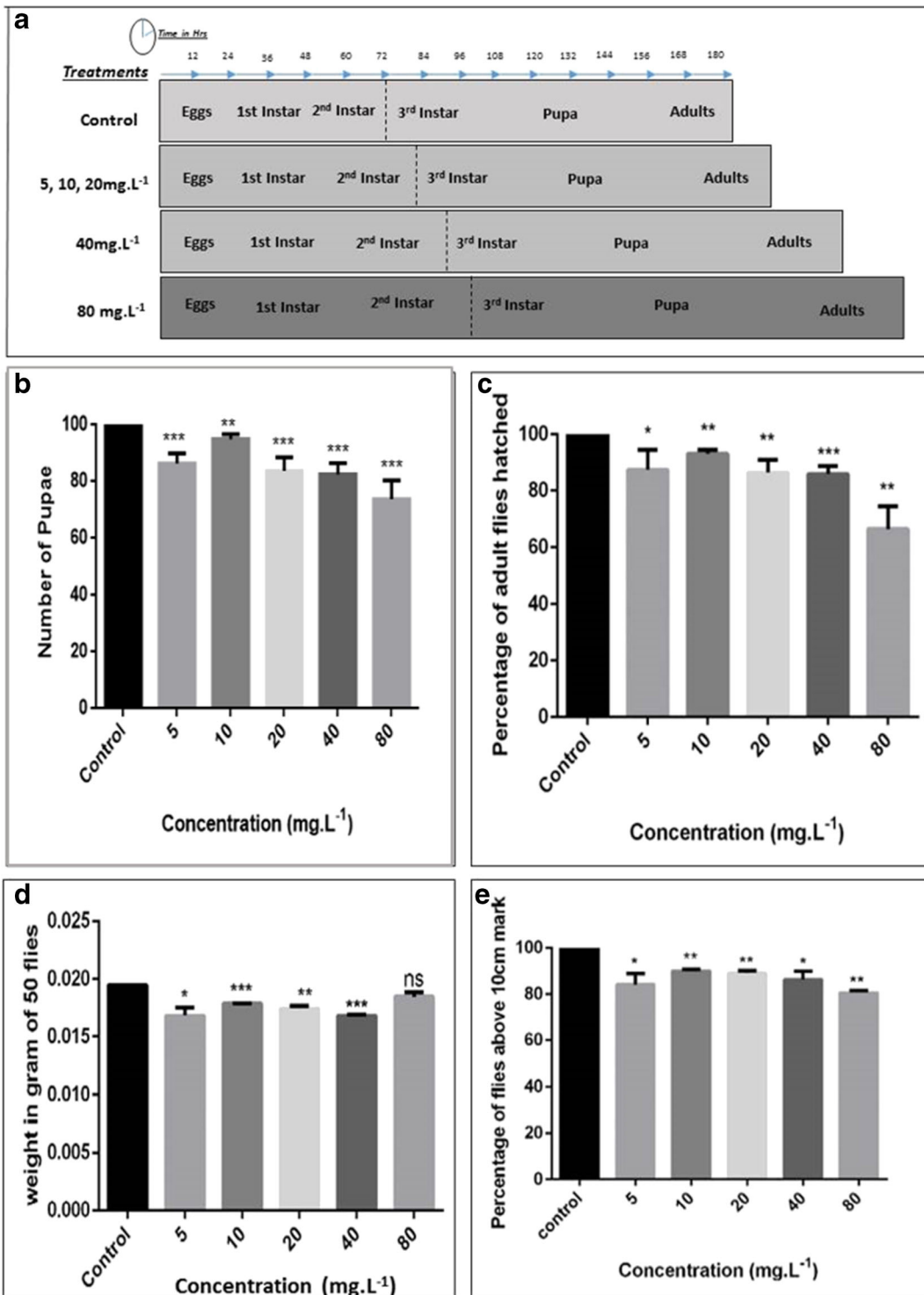
The increased use of HApNPs in biomedical applications has raised great concern about its potential risk to human health. Several reports suggest size, morphology and structure of HApNPs have significant effects on biological responses. Zhao et al. reports the synthesis of needle-, rod-, sphere- and plate-shaped HApNPs and their cytotoxicity on human cells. According to their findings, the needle- and plate-shaped HApNPs are responsible for most significant cell death in comparison with the other two NPs. Furthermore, Loo et al. has synthesized needle- and rod-shaped HApNPs and studied the toxicity of the NPs. Keeping those results into account, the present study focuses on the synthesis of rod-shaped HApNPs to study the toxicity. (Zhao et al. 2013a, b) HApNP treatment causes delay in development at higher concentration. Developmental delay is associated with a disturbance in the oogenesis period, ovarian defect and delayed egg chamber development. Nanoparticles like Fe, Ca, Cu and Ag are previously reported to cause such developmental delay in *Drosophila* (Chen et al. 2015; Gorth et al. 2011). NPs due to its small size can easily pass through the placental barrier (Chu et al. 2010) and tend to cause cellular and oxidative damage to DNA (Bhabra et al. 2009). In the current study, developmental delay is observed from larvae to the adult stage.

Larva crawling experiment is considered as a gauge to monitor the functionality of neurons (Kitamoto 2001; Pulver et al. 2009). Previously, silica nanoparticles have been reported to interfere with the neuronal cells, cause toxicity and affect the calcium homeostasis (Ariano et al. 2011). The larvae crawling experiment points that with an increase of HApNP treatment, the crawling speed decreases. The track made by the HApNP-treated larvae evidenced that HApNP induces confusing behaviour, leading to more sharp turns, non-linear crawling and lesser crawling speed. The crawling speed of wild-type third instar larvae is about 6–8 cm min⁻¹ (Chyb and Gompel 2013). The slower speed and more turns could be due to damage in the sub-oesophageal ganglion and poor coordination between the brain and the mechanosensory neurons (Riedl and Louis 2012). A similar larva crawling defect is reported with the

treatment of titania, silica, gold and carbon nanoparticles (Han et al. 2014; Liu et al. 2009; Raj et al. 2016; Sabat et al. 2016).

Nanoparticles such as silver, gold and titanium cause oxidative stress, by the generation of more amount of ROS (Ong et al. 2016). NBT assay is a known method to detect the amount of ROS (Sabat et al. 2016; Ahamed et al. 2010). In the current study, after HApNP treatment, oxidative damage occurred, which is detected by NBT assay. The amount of oxidative stress generated at lower concentration, i.e. 5 mg L⁻¹ of HApNP is comparatively more than that of highest one, i.e. 80 mg L⁻¹. The lower amount of ROS at higher concentration could be due to agglomeration of the nanoparticles (Yang et al. 2012). Due to agglomeration, NP loses its small size and larger surface area (Bose and Saha 2003) resulting in less production of ROS. A similar mechanism is reported in the case of cerium oxide NP treated to *Drosophila* (Alaraby et al. 2015). Nanoparticles produce oxidative stress in a cell by several means (Xia et al. 2008; Kim et al. 2009; Li et al. 2008). One of the possible mechanisms is the endocytosis-mediated mechanism in the acidic pH of the lysosome, which triggers a lysosome-enhanced Trojan horse effect resulting release of toxic ions. These ions cause toxicity to several cell organelles and result oxidative stress (Sabella et al. 2014; Manke et al. 2013). Since the foregut of *Drosophila* has acidic pH, a similar mechanism is anticipated with exposure after HApNPs.

To check whether oxidative damage leads to cellular damage or not, trypan blue staining was performed. Trypan blue staining depicts highest dead cells in the gut treated with the lowest concentration of HApNPs. To check the effect of HApNPs in cellular pathways, larval gut was checked under scanning electron microscope. Surprisingly, the amount of phosphorus decreased from the gut after the treatment of low concentration of HApNPs indicating that it affects the phosphorous absorption (Heaney and Nordin 2002). Similarly, the amount of calcium found to be decreased in case of lower concentration treated samples whereas it steadily increases from 40 mg L⁻¹ concentration onwards. Now the question that arises is why low supplementation of HApNPs decreases the level of calcium and phosphate within the gut? The possible explanation could be when the concentration of NP is low; probably the NPs can easily penetrate through the gut epithelium and enter into the hemolymph, resulting in no calcium inside the gut. However, at high concentration, due to



◀ **Fig. 5** Assessment of lifecycle, adults and behaviour (a). The lifecycle of various concentration of HApNP-treated flies. From 5, 10 and 20 mg L⁻¹ vial, a delay of 12 h in third instar larvae formation was found in comparison to control. At higher concentration of 40 and 80 mg L⁻¹, a delay of 18 and 24 h was observed respectively. **b** Percentage of pupae formed from third instar larvae in different concentration of HApNP-treated vial. The level of significance was marked in comparison with the control. (***P* value = 0.0014, ****P* value <0.0007). **c** Percentage of adult flies hatched from pupae in each concentration of HApNP-treated vials are plotted with respected to the control flies. The level of significance was marked in comparison with the control (**P* value = 0.0372, ****P* value = 0.0010, ***P* value <0.007). **d** Weight of adult flies: The total weight of 25 males and 25 females is plotted with respect to its corresponding concentration. The levels of significance were marked in comparison with the control (**P* value = 0.0328, ***P* value = 0.0073, ****P* value <0.0005, ns = 0.05). **e** Climbing behaviour: The percentage of flies that climb in 5 and 80 mg L⁻¹ vial was significantly lower in comparison to control. The climbing of flies in 10, 40 and 80 mg L⁻¹ treatment was found to be decreasing but were less affected in comparison to control (**P* value <0.04, ***P* value <0.004)

agglomeration, the particle size increases, and the HApNP stays inside the gut resulting increase in calcium and phosphorus within the gut which occurs after 40 mg L⁻¹ onwards. Does the change in the percentage of calcium and phosphate interfere with the normal activity of the cell? To check this structure of the gut cell was overviewed. The *Drosophila* gut is lined with the single-layered epithelial cell. To check if there is any nuclear damage in the gut cells, the gut was stained with DAPI. In treated samples, clustered small nucleus and micronuclei-like structures were observed in the gut epithelium. This might be due to apoptosis of the gut cells which is pretty obvious in the late third instar larvae as during pupae formation, the whole larval gut will disintegrate and will ultimately be replaced by the adult gut. Since such structures are not observed in the case of the control, we anticipate that HApNP induces apoptosis in larval gut earlier than its actual time resulting developmental delay and abnormal phenotypes. Although no such report is available in the literature from in vivo study, the in vitro study reports HApNP as a known inducer of apoptosis in osteoblasts and human hepatoma cells (Shi et al. 2009; Yuan et al. 2010).

At higher concentration of HApNP treatment, developmental delay was observed along with less number of pupae count. The decreased pupae count is a direct consequence of NP egg-pupae

developmental delay (Panacek et al. 2011; Ong et al. 2016). Highest decrease in pupae count (66%) is observed in 80 mg L⁻¹ concentration vial. At 80 mg L⁻¹, agglomeration of NP is occurring resulting a delay in the pupae-adult development. A similar abnormal delay in pupae-adult transition is reported from nanoparticles like Ca, Cu, and Fe (Chen et al. 2015; Gorth et al. 2011). Besides developmental delay, climbing behaviour was also found to be affected in the adult flies which are associated with the functionality of antenna. Behavioural assay specifies that with an increase of HApNP treatment, flies become more positive geotropic. This further suggests that HApNP exposure induces positive geotaxis suggesting the possibility of a defective antenna. This result is in agreement with the earlier report where oral ingestion of carbon, silver and gold nanoparticles resulted anomaly in developmental and behavioural defect (Key et al. 2011; Liu et al. 2009; Raj et al. 2016).

An antenna is the largest mechano-sensory organ of the fly. Besides antennae, bristles also contribute for the mechanosensation. In HApNPs treated adults, abnormal bristles were observed in the thorax region (Mackay 1995). In different concentration, aSC, pSC, aDC and pDC bristles were missing. The arrangement of bristles on the thorax is regulated by several genes and signalling pathways (Peña-Rangel et al. 2002; Culi et al. 2001). One of the major genes which is involved in the development of bristles is *achaete-scute* complex (Georgiev and Gerasimova 1992). Thus, any mutation in this family of genes during the pupae-adult development will result in bristle abnormality. Furthermore, EGFR and Notch signalling pathway also play a role in bristle development (Furman and Bukharina 2007). Missing bristle in HApNP treated flies indicates an anomaly in the regulation of above two pathways.

Besides bristle, HApNP also induces wing phenotype (incomplete venations) at a lower concentration. An incomplete venation is the result of idiosyncrasy in the wing imaginal disk during the metamorphosis (de Celis 2003). A mutation in the posterior cross vein (PCV) gene induces similar abnormal wing pattern. Besides PCV, signalling pathways like bone morphogenic protein (BMP) and Notch also affect the spacing and marginal fate of the wing pattern (de Celis 2003). Thus, any interference with either of these pathways will result in an abnormal wing phenotype. Besides venation

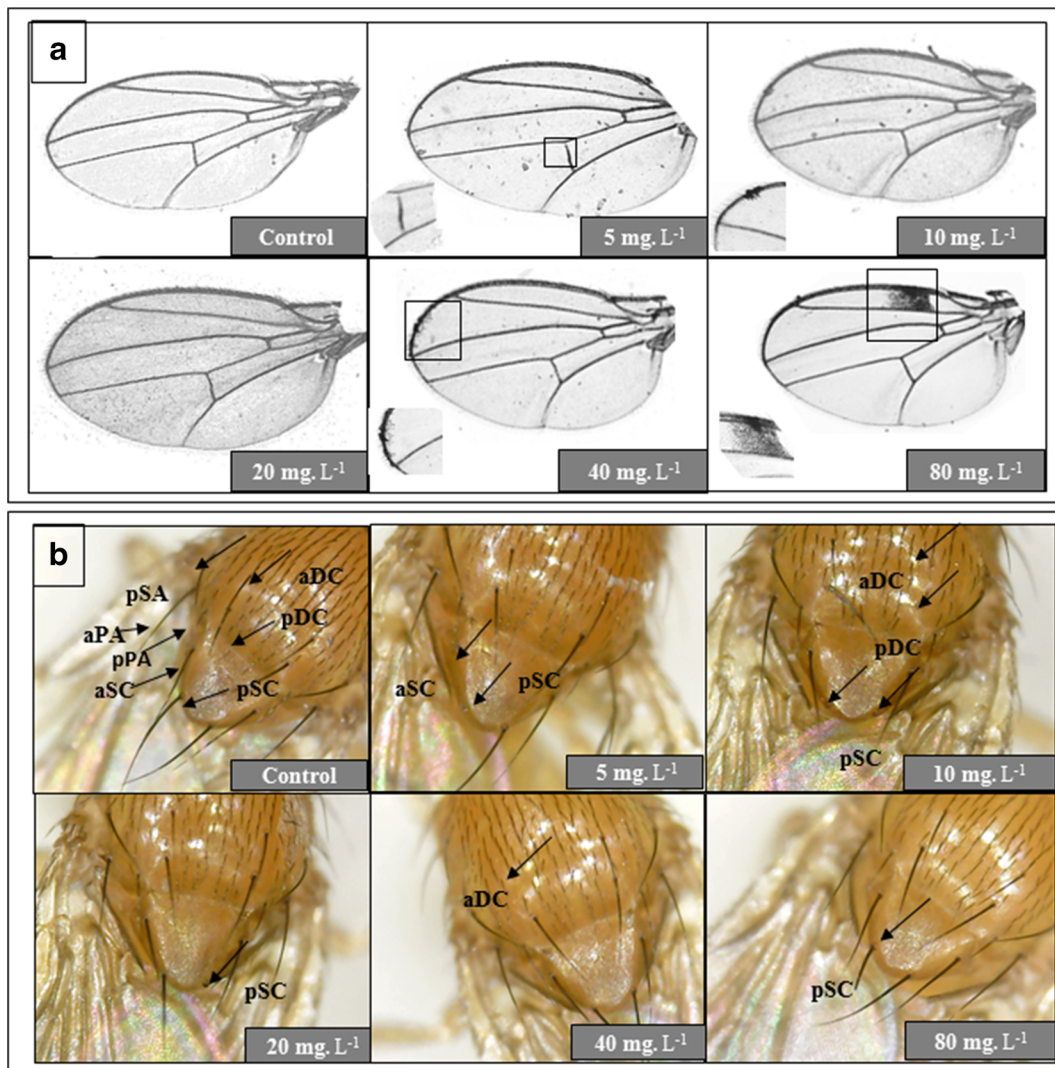


Fig. 6 Bristle and wing phenotype. **a** Control shows the normal wing venation in *Drosophila*. In 5 mg L^{-1} , the posterior cross vein is discontinuous. The abnormality is indicated by a *black square*. In 10, 40, and 80 mg L^{-1} , there is a formation of brown patches due to thick wing hairs. The magnified patches are shown in the *inset* below the actual image. **b** Control shows the regular distribution of bristles in the thorax. In 5 mg L^{-1} , there is loss of left aSC, left pSC, and left aDC bristles. Ten milligrams per liter shows

loss of right aDC, right pDC, and both the left and right pSC bristles. In 20 mg L^{-1} , there is no right pSC bristle. Forty milligrams per liter shows loss of left aDC bristle. In 80 mg L^{-1} , there is broken pSC bristle. The *black arrow* points to the missing or affected bristle. aDC anterior dorso-central, pDC posterior dorso-central, aSC anterior scutellar, pSC posterior scutellar, pPA posterior post-alar, aPA anterior post-alar, pSA posterior supra-alar

defect, brown patches were found on the wing surface due to the formation of comparatively thicker wing hairs. The wing hairs of *Drosophila* are composed of actin (Ren et al. 2006; Fristrom et al. 1993). During wing development, the thickness and organization of wing hair depends on the planar polarization of cells and the amount of actin present in the hair (Eaton et al. 1996). The formation of brown patches in the wing

indicates the HApNPs induces defective planar cell polarity in the wing. Besides wings, the eye size also seems to be affected and irregular margins are found in the eye along with damaged ommatidia. Finally, we checked the survivability of the flies in order to check the response of the adults towards stress (Grover et al. 2009). HApNP-treated flies were less resistant to stress and thus died earlier than the control flies when treated

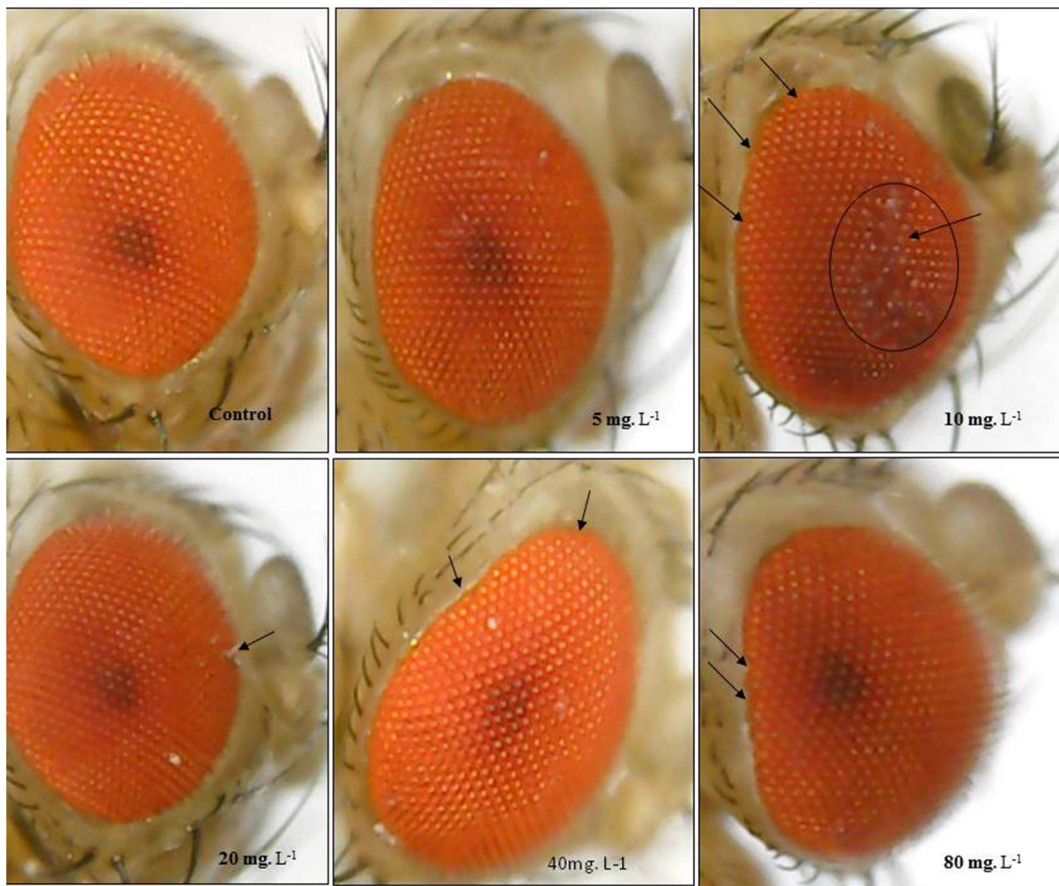


Fig. 7 Eye phenotype: the eyes of adult flies of different treated concentration are imaged and the damaged areas are shown by an *arrow*. The *big circle* shows the damaged ommatidia and the *arrows* show the irregular margin of the eye

with hydrogen peroxide. All the phenotypic defects handicap the treated flies to perform better during stress condition.

Conclusion

These findings collectively point to the fact that HApNPs can distress the neuronal development and behaviour of *Drosophila* in a concentration-dependent manner. HApNPs bring these variations dramatically by altering the amount of calcium and phosphorus within the gut, increasing the ROS, and by inducing the apoptosis within the gut. Although HApNP is widely used to deliver various drugs and in dental purposes, only very few studies focuses on the toxic property of this NPs and its effect on development. The developmental and behavioural defects observed in the current study is a clear consequence of alteration of signalling pathways

during development as well as the alteration of the amount of calcium and phosphorus during the developmental process. The toxic effect caused by HApNPs described herein needs further investigation. How

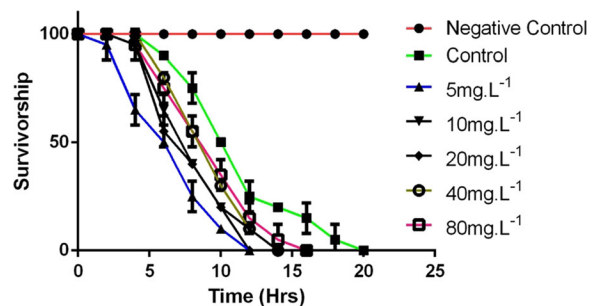


Fig. 8 Survivorship assay: the control and HApNP-treated flies were exposed to 5% sucrose and 10% H₂O₂. In 5 and 10 mg L⁻¹, the HAp-treated flies died within 12 h, whereas in 20, 40, and 80 mg L⁻¹-treated vials, flies died gradually within 14 and 16 h. The control flies could endure the stress up to 20 h and in negative control, all the flies were alive for more than 24 h

HApNPs interfere with the imaginal disc, a polar organization of cells and bring structural and functional variation, will be the focus of our further investigations.

Acknowledgements S.A. Pappus is thankful to DST-Inspire fellowship for the financial support he received to carry out this work. Two anonymous reviewers are thankfully acknowledged for their valuable comments, which help to improve the manuscript.

Compliance with ethical standards

Conflict of interest The authors declare that they have no conflict of interest.

References

- Ahamed M, Posgai R, Gorey TJ, Nielsen M, Hussain SM, Rowe JJ (2010) Silver nanoparticles induced heat shock protein 70, oxidative stress and apoptosis in *Drosophila melanogaster*. *Toxicol Appl Pharmacol* 242(3):263–269
- Alaraby M, Hernández A, Annangi B, Demir E, Bach J, Rubio L, Creus A, Marcos R (2015) Antioxidant and antigenotoxic properties of CeO₂ NPs and cerium sulphate: studies with *Drosophila melanogaster* as a promising in vivo model. *Nanotoxicology* 9(6):749–759
- Albanese A, Tang PS, Chan WC (2012) The effect of nanoparticle size, shape, and surface chemistry on biological systems. *Annu Rev Biomed Eng* 14:1–16
- Ariano P, Zamburlin P, Gilardino A, Mortera R, Onida B, Tomatis M, Ghiazza M, Fubini B, Lovisolo D (2011) Interaction of spherical silica nanoparticles with neuronal cells: size-dependent toxicity and perturbation of calcium homeostasis. *Small* 7(6):766–774
- Bhabra G, Sood A, Fisher B, Cartwright L, Saunders M, Evans WH, Surprenant A, Lopez-Castejon G, Mann S, Davis SA (2009) Nanoparticles can cause DNA damage across a cellular barrier. *Nat Nanotechnol* 4(12):876–883
- Bose S, Saha SK (2003) Synthesis and characterization of hydroxyapatite nanopowders by emulsion technique. *Chem Mater* 15(23):4464–4469
- Campos-Ortega JA, Hartenstein V (2013) The embryonic development of *Drosophila melanogaster*. Springer Science & Business Media,
- Carmona ER, Escobar B, Vales G, Marcos R (2015) Genotoxic testing of titanium dioxide anatase nanoparticles using the wing-spot test and the comet assay in *Drosophila*. *Mutation Research/Genetic Toxicology and Environmental Mutagenesis* 778:12–21
- de Celis JF (2003) Pattern formation in the *Drosophila* wing: the development of the veins. *BioEssays* 25(5):443–451
- Chaudhry AA, Haque S, Kellici S, Boldrin P, Rehman I, Khalid FA, Darr JA (2006) Instant nano-hydroxyapatite: a continuous and rapid hydrothermal synthesis. *Chem Commun* 21: 2286–2288
- Chen Y-H, Liu H-P, Chen H-Y, Tsai F-J, Chang C-H, Lee Y-J, Lin W-Y, Chen W-C (2011) Ethylene glycol induces calcium oxalate crystal deposition in Malpighian tubules: a drosophila model for nephrolithiasis/urolithiasis. *Kidney Int* 80(4):369–377
- Chen H, Wang B, Feng W, Du W, Ouyang H, Chai Z, Bi X (2015) Oral magnetite nanoparticles disturb the development of *Drosophila melanogaster* from oogenesis to adult emergence. *Nanotoxicology* 9(3):302–312
- Chi T, Kim MS, Lang S, Bose N, Kahn A, Flechner L, Blaschko SD, Zee T, Muteliefu G, Bond N (2015) A *Drosophila* model identifies a critical role for zinc in mineralization for kidney stone disease. *PLoS One* 10(5):e0124150
- Cho K, Wang X, Nie S, Chen ZG, Shin DM (2008a) Therapeutic nanoparticles for drug delivery in cancer. *Clin Cancer Res* 14(5):1310–1316. doi:10.1158/1078-0432.CCR-07-1441
- Cho K, Wang X, Nie S, Shin DM (2008b) Therapeutic nanoparticles for drug delivery in cancer. *Clin Cancer Res* 14(5): 1310–1316
- Chu M, Wu Q, Yang H, Yuan R, Hou S, Yang Y, Zou Y, Xu S, Xu K, Ji A (2010) Transfer of quantum dots from pregnant mice to pups across the placental barrier. *Small* 6(5):670–678
- Chyb S, Gompel N (2013) Atlas of *Drosophila* morphology: wild-type and classical mutants. Academic Press
- Cohen CA, Karfakis JA, Kurnick MD, Rzigalinski B (2008) Cerium oxide nanoparticles reduce free radical-mediated toxicity in *Drosophila melanogaster*. *FASEB J* 22(1 Supplement):624.621–624.621
- Culi J, Martín-Blanco E, Modolell J (2001) The EGF receptor and N signalling pathways act antagonistically in *Drosophila* mesothorax bristle patterning. *Development* 128(2):299–308
- Demir E, Vales G, Kaya B, Creus A, Marcos R (2011) Genotoxic analysis of silver nanoparticles in *Drosophila*. *Nanotoxicology* 5(3):417–424
- Dominick OS, Truman JW (1986) The physiology of wandering behaviour in *Manduca sexta*. III Organization of wandering behaviour in the larval nervous system *Journal of experimental biology* 121(1):115–132
- Dorozhkin SV (2010) Nanosized and nanocrystalline calcium orthophosphates. *Acta Biomater* 6(3):715–734
- Duer MJ, Friščić T, Proudfoot D, Reid DG, Schoppet M, Shanahan CM, Skepper JN, Wise ER (2008) Mineral surface in calcified plaque is like that of bone. *Arterioscler Thromb Vasc Biol* 28(11):2030–2034
- Eaton S, Wepf R, Simons K (1996) Roles for Rac1 and Cdc42 in planar polarization and hair outgrowth in the wing of *Drosophila*. *J Cell Biol* 135(5):1277–1289
- Evan AP (2010) Physiopathology and etiology of stone formation in the kidney and the urinary tract. *Pediatr Nephrol* 25(5): 831–841
- Evan AP, Lingeman JE, Coe FL, Worcester EM (2008) Role of interstitial apatite plaque in the pathogenesis of the common calcium oxalate stone. *Semin Nephrol* 28(2):111–119
- Fristrom D, Wilcox M, Fristrom J (1993) The distribution of PS integrins, laminin a and F-actin during key stages in *Drosophila* wing development. *Development* 117(2):509–523
- Furman D, Bukharina T (2007) Genetic control of bristle pattern formation in *Drosophila melanogaster*. *Dokl Biol Sci* 417: 484–486

- Georgiev P, Gerasimova T (1992) Genes involved in the development of bristles and hairs in *Drosophila melanogaster*. *Genetica* 87(1):31–35
- Gorth DJ, Rand DM, Webster TJ (2011) Silver nanoparticle toxicity in *Drosophila*: size does matter. *Int J Nanomedicine* 6: 343–350
- Grover D, Ford D, Brown C, Hoe N, Erdem A, Tavaré S, Tower J (2009) Hydrogen peroxide stimulates activity and alters behavior in *Drosophila melanogaster*. *PLoS One* 4(10):e7580
- Han X, Geller B, Moniz K, Das P, Chippindale AK, Walker VK (2014) Monitoring the developmental impact of copper and silver nanoparticle exposure in *Drosophila* and their microbiomes. *Sci Total Environ* 487:822–829
- Heaney RP, Nordin B (2002) Calcium effects on phosphorus absorption: implications for the prevention and co-therapy of osteoporosis. *J Am Coll Nutr* 21(3):239–244
- Hirata T, Cabrero P, Berkholz DS, Bondeson DP, Ritman EL, Thompson JR, Dow JA, Romero MF (2012) In vivo *Drosophila* genetic model for calcium oxalate nephrolithiasis. *American Journal of Physiology-Renal Physiology* 303(11):F1555–F1562
- Jambunathan N (2010) Determination and detection of reactive oxygen species (ROS), lipid peroxidation, and electrolyte leakage in plants. *Plant stress tolerance: methods and protocols*:291–297
- Jiang Z, Asplin JR, Evan AP, Rajendran VM, Velazquez H, Nottoli TP, Binder HJ, Aronson PS (2006) Calcium oxalate urolithiasis in mice lacking anion transporter *Slc26a6*. *Nat Genet* 38(4):474–478
- Kalita SJ, Bhardwaj A, Bhatt HA (2007) Nanocrystalline calcium phosphate ceramics in biomedical engineering. *Mater Sci Eng C* 27(3):441–449
- Kantharia N, Naik S, Apte S, Kheur M, Kheur S, Kale B (2014) Nano-hydroxyapatite and its contemporary applications. *Bone* 34(15.2):1.71
- Key SCS, Reaves D, Turner F, Bang JJ (2011) Impacts of silver nanoparticle ingestion on pigmentation and developmental progression in *Drosophila*. *Atlas J Biol* 1(3):52–61
- Kim S, Choi JE, Choi J, Chung K-H, Park K, Yi J, Ryu D-Y (2009) Oxidative stress-dependent toxicity of silver nanoparticles in human hepatoma cells. *Toxicol in Vitro* 23(6):1076–1084
- Kitamoto T (2001) Conditional modification of behavior in *Drosophila* by targeted expression of a temperature-sensitive shibire allele in defined neurons. *J Neurobiol* 47(2):81–92
- Krebs RA, Feder ME (1997) Tissue-specific variation in Hsp70 expression and thermal damage in *Drosophila melanogaster* larvae. *J Exp Biol* 200(14):2007–2015
- LeGeros R (1991) Biologically relevant calcium phosphates: preparation and characterisation, calcium phosphates in oral biology and medicine. Karger, Basel
- Li N, Xia T, Nel AE (2008) The role of oxidative stress in ambient particulate matter-induced lung diseases and its implications in the toxicity of engineered nanoparticles. *Free Radic Biol Med* 44(9):1689–1699
- Liu X, Vinson D, Abt D, Hurt RH, Rand DM (2009) Differential toxicity of carbon nanomaterials in *Drosophila*: larval dietary uptake is benign, but adult exposure causes locomotor impairment and mortality. *Environmental science & technology* 43(16):6357–6363
- Ma G, Liu XY, Wang M (2011) Growth and mechanisms of enamel-like hierarchical nanostructures on single crystalline hydroxyapatite micro-ribbons. *J Nanosci Nanotechnol* 11(6): 5199–5206
- Mackay TF (1995) The genetic basis of quantitative variation: numbers of sensory bristles of *Drosophila melanogaster* as a model system. *Trends Genet* 11(12):464–470
- Manke A, Wang L, Rojanasakul Y (2013) Mechanisms of nanoparticle-induced oxidative stress and toxicity. *Biomed Res Int* 2013:942916
- Mostafa NY, Brown PW (2007) Computer simulation of stoichiometric hydroxyapatite: structure and substitutions. *J Phys Chem Solids* 68(3):431–437
- MuÈller RH, MaÈder K, Gohla S (2000) Solid lipid nanoparticles (SLN) for controlled drug delivery—a review of the state of the art. *Eur J Pharm Biopharm* 50(1):161–177
- Nichols CD, Becnel J, Pandey UB (2012) Methods to assay *Drosophila* behavior. *JoVE (Journal of Visualized Experiments)* 61:e3795–e3795
- Ong C, Yung L-YL, Cai Y, Bay B-H, Baeg G-H (2015) *Drosophila melanogaster* as a model organism to study nanotoxicity. *Nanotoxicology* 9(3):396–403
- Ong C, Lee QY, Cai Y, Liu X, Ding J, Yung L-YL, Bay B-H, Baeg G-H (2016) Silver nanoparticles disrupt germline stem cell maintenance in the *Drosophila* testis. *Scientific reports* 6
- Panacek A, Pucek R, Safarova D, Dittrich M, Richtrova J, Benickova K, Zboril R, Kvittek L (2011) Acute and chronic toxicity effects of silver nanoparticles (NPs) on *Drosophila melanogaster*. *Environmental science & technology* 45(11): 4974–4979
- Pandey UB, Nichols CD (2011) Human disease models in *Drosophila melanogaster* and the role of the fly in therapeutic drug discovery. *Pharmacol Rev* 63(2):411–436
- Pandey A, Chandra S, Chauhan LKS, Narayan G, Chowdhuri DK (2013) Cellular internalization and stress response of ingested amorphous silica nanoparticles in the midgut of *Drosophila melanogaster*. *Biochimica et Biophysica Acta (BBA)-General Subjects* 1830(1):2256–2266
- Peña-Rangel MT, Rodriguez I, Riesgo-Escovar JR (2002) A misexpression study examining dorsal thorax formation in *Drosophila melanogaster*. *Genetics* 160(3):1035–1050
- Pompa PP, Vecchio G, Galeone A, Brunetti V, Sabella S, Maiorano G, Falqui A, Bertoni G, Cingolani R (2011) In vivo toxicity assessment of gold nanoparticles in *Drosophila melanogaster*. *Nano Res* 4(4):405–413
- Pulver SR, Pashkovski SL, Hornstein NJ, Garrity PA, Griffith LC (2009) Temporal dynamics of neuronal activation by Channelrhodopsin-2 and TRPA1 determine behavioral output in *Drosophila* larvae. *J Neurophysiol* 101(6):3075–3088
- Puvvada N, Panigrahi PK, Pathak A (2010) Room temperature synthesis of highly hemocompatible hydroxyapatite, study of their physical properties and spectroscopic correlation of particle size. *Nano* 2(12):2631–2638
- Raj A, Shah P, Agrawal N (2016) Ingestion of gold nanoparticles (AuNPs) affects survival in *Drosophila* in a dose-dependent manner. *Int J Sci Res* 5(6)
- Reddy LH, Arias JL, Nicolas J, Couvreur P (2012) Magnetic nanoparticles: design and characterization, toxicity and biocompatibility, pharmaceutical and biomedical applications. *Chem Rev* 112(11):5818–5878

- Ren N, He B, Stone D, Kirakodu S, Adler PN (2006) The shavenoid gene of *Drosophila* encodes a novel actin cytoskeleton interacting protein that promotes wing hair morphogenesis. *Genetics* 172(3):1643–1653
- Riedl J, Louis M (2012) Behavioral neuroscience: crawling is a no-brainer for fruit fly larvae. *Curr Biol* 22(20):R867–R869
- Ryall RL (2008) The future of stone research: rummagings in the attic, Randall's plaque, nanobacteria, and lessons from phylogeny. *Urol Res* 36(2):77–97
- Sabat D, Patnaik A, Ekka B, Dash P, Mishra M (2016) Investigation of titania nanoparticles on behaviour and mechanosensory organ of *Drosophila melanogaster*. *Physiol Behav* 167:76–85
- Sabella S, Carney RP, Brunetti V, Malvindi MA, Al-Juffali N, Vecchio G, Janes SM, Bakr OM, Cingolani R, Stellacci F (2014) A general mechanism for intracellular toxicity of metal-containing nanoparticles. *Nano* 6(12):7052–7061
- Shi Z, Huang X, Cai Y, Tang R, Yang D (2009) Size effect of hydroxyapatite nanoparticles on proliferation and apoptosis of osteoblast-like cells. *Acta Biomater* 5(1):338–345
- Slowing II, Vivero-Escoto JL, Wu C-W, Lin VS-Y (2008) Mesoporous silica nanoparticles as controlled release drug delivery and gene transfection carriers. *Adv Drug Deliv Rev* 60(11):1278–1288
- Sun L, Berndt CC, Gross KA, Kucuk A (2001) Material fundamentals and clinical performance of plasma-sprayed hydroxyapatite coatings: a review. *J Biomed Mater Res* 58(5): 570–592
- Vales G, Demir E, Kaya B, Creus A, Marcos R (2013) Genotoxicity of cobalt nanoparticles and ions in *Drosophila*. *Nanotoxicology* 7(4):462–468
- Vecchio G, Galeone A, Brunetti V, Maiorano G, Rizzello L, Sabella S, Cingolani R, Pompa PP (2012) Mutagenic effects of gold nanoparticles induce aberrant phenotypes in *Drosophila melanogaster*. *Nanomedicine: Nanotechnology, Biology and Medicine* 8(1):1–7
- Xia T, Kovochich M, Liang M, Mädler L, Gilbert B, Shi H, Yeh JI, Zink JI, Nel AE (2008) Comparison of the mechanism of toxicity of zinc oxide and cerium oxide nanoparticles based on dissolution and oxidative stress properties. *ACS Nano* 2(10):2121–2134
- Yang Y, Oztekin A, Neti S, Mohapatra S (2012) Particle agglomeration and properties of nanofluids. *J Nanopart Res* 14(5):1–10
- Yao J, Tjandra W, Chen YZ, Tam KC, Ma J, Soh B (2003) Hydroxyapatite nanostructure material derived using cationic surfactant as a template. *J Mater Chem* 13(12):3053–3057
- Yuan Y, Liu C, Qian J, Wang J, Zhang Y (2010) Size-mediated cytotoxicity and apoptosis of hydroxyapatite nanoparticles in human hepatoma HepG2 cells. *Biomaterials* 31(4):730–740
- Zhao X, Ng S, Heng BC, Guo J, Ma L, Tan TTY, Ng KW, Loo SCJ (2013a) Cytotoxicity of hydroxyapatite nanoparticles is shape and cell dependent. *Arch Toxicol* 87(6):1037–1052
- Zhao X, Ong KJ, Ede JD, Stafford JL, Ng KW, Goss GG, Loo SCJ (2013b) Evaluating the toxicity of hydroxyapatite nanoparticles in catfish cells and zebrafish embryos. *Small* 9(9–10): 1734–1741